https://doi.org/10.5194/egusphere-2023-2715
Preprint. Discussion started: 21 November 2023

Dynamic Response of Pile-Slab Retaining Wall Structure under Rockfall Impact

Peng Zou[1, 2 , 3], Gang Luo[1, *], Yuzhang Bi[4], Hanhua Xu[2, 3]

1. *Faculty of Geosciences and Environmental Engineering, Southwest Jiaotong University, Chengdu 611756, China*

22. *Kunming Prospecting Design Institute of China Nonferrous Metals Industry Co., Ltd, Yunnan 650051, Chin*a

3. *Key Laboratory of Geotechnical Engineering and Geohazards, Yunnan, 650051, China*

4. *College of Civil Engineering, Fuzhou University., Fuzhou 350000, China*

***Corresponding author at:** Faculty of Geosciences and Environmental Engineering, Southwest Jiaotong University, Chengdu 611756, China

E-mail addresses: luogang@home.swjtu.edu.cn (G. Luo).

https://doi.org/10.5194/egusphere-2023-2715
Preprint. Discussion started: 21 November 2023

Abstract: The numerical experiments investigate the dynamic response of a pile-slab retaining wall under the impact of rockfall. Firstly, a full-scale numerical model of a four-span pile-slab retaining wall satisfying specification requirements is established. Secondly, the numerical experiments investigate the dynamic response of a pile-slab retaining wall under different impact centers and velocities. Finally, the maximum impact energy that the structure can resist is predicted. Results reveal that: (1) During the impact process, the stress, strain, and concrete damage of the structure gradually spread from the impact center to the entire structure and ultimately result in permanent deformation; (2) The lateral displacement of pile at ground surface and the number of damage failure units under the pile as the impact center is greater than those under the slab as impact center. It shows that the impact position has a significant effect on the stability of the structure.(3) The impact force, interaction force, lateral dispalcement of pile at ground surface, and concrete damage is increased with the increase of impact velocity. Under pile as the impact center (slab as the impact center), when the velocity increases from 15m/s to 30m/s, the impact force increases by 1.42, 1.91, and 2.41 times (1.41, 1.90, and 2.41 times), the interaction force increases by 1.25, 1.47, and 1.68 times (1.24, 1.47, and 1.68 times), and the maximum lateral displacement of pile at ground surface increases by 1.57, 2.24, and 3 times (1.55, 2.23, and 3 times). (4) Utilizing this relationship btween the impact velocity and the maximum lateral displacement of pile at ground surface, the estimated maximum impact energy that the pile-slab retaining wall can withstand is 905 kJ in this study when the structure top is taken as the impact point. Impact resistance of the structure optimized 1.814 times compared to traditional reinforced concrete retaining walls.

Keywords: rockfall, pile-slab retaining wall, numerical simulation, dynamic response

List of symbols

P	Actual lateral soil resistance (kPa).	F_{dm}	Peak impact force (kN).
P_{u}	Ultimate lateral soil resistance (kPa).	F_{im}	Peak interaction force (kN).
$S_{\mathrm{u\_cu}}$	Consolidated isotropic undrained tri-axial shear strength of soil (kPa/m).	α	Ratio of the peak impact force to the peak interaction force (%).
y	Actual lateral soil deformation (m).	S_{mpt}	Maximum the lateral displacement of pile at the ground surface at t = 650 ms (mm).
B	Pile width (m).	N_d	Number of damage failure units.
z	Depth below the soil surface (m).	β	Ratio of damage failure units to overall structure units (%).

https://doi.org/10.5194/egusphere-2023-2715
Preprint. Discussion started: 21 November 2023

S_p	Shape correction factor of pile section.	m	Impactor mass (kg).
E	Initial kinetic energy of impactor.	v	Initial velocity of impactor (m/s).

1. Introduction

Rockfall disaster are a great threat to roads, railways, buildings and inhabitants in mountainous terrain (Hungr et al., 2014; Crosta and Agliardi, 2004; Shen et al., 2019). It can be described as a process that the quick bouncing, rolling and sliding movement of one (or several) boulders down a slope (Peila and Ronco, 2009). The velocity values range from a few metres per second to up to 30 m (Giani, 1992). Muraishi et al. (2005) surveyed 607 rockfall events found that about 68% of rockfall events have an impact energy of less than 100 kJ, whereas 90% have less than 1000 kJ. The study of Chau et al. (2002) shows that the rotational kinetic energy of rockfall only accounts for 10% of the total kinetic energy. To prevent such geological hazards, scholars and engineers have proposed different types of technical solutions. Two primary categories of defensive measures are commonly employed: active and passive. Active protection measures mainly include: masonry protection, reinforcement protection (grouting, anchor rod, and anchor cable), initiative protective net, etc (Yang et al., 2019). Passive protection measures include: passive flexible protection (Yu et al., 2021), rockfall shed gallery (Zhao et al., 2018), rockfall retaining wall, etc. Considering many factors such as technology and economy, rockfall retaining wall is often used in practical engineerin (Volkwein et al., 2011).

Currently, there are various types of retaining walls employed in engineering projects for the purpose of rockfall interception, including masonry retaining walls, reinforced concrete (RC) retaining walls, reinforced soil retaining walls, and pile-slab retaining walls (PSRW). The cross-section of masonry retaining walls resembles that of gravity retaining walls. Due to inherent structural weakness of these walls, their ability to absorb the impact energy from rockfall is limited (Mavrouli et al., 2017). To enhance the impact resistance, the reinforced concrete retaining walls have been utilized (Yong et al., 2020). These structures can intercept rockfall impact energy ranging approximately from 120 to 500 kJ (Maegawa et al., 2011). To prevent concrete from being damaged by the direct impact of rockfall, a buffer layer is generally added in front of the structure for protection, such as reinforced soil and gabion cushion (Perera et al., 2021). Although the impact

https://doi.org/10.5194/egusphere-2023-2715
Preprint. Discussion started: 21 November 2023

resistance of the structure has been improved, there is still a problem of limited interception height. When the required interception height is large, the foundation size has to be increased to prevent the structures from overturning. In order to mitigate against rockfall events involving higher energy levels, numerous researchers have proposed the implementation of reinforced soil retaining walls. Extensive studies have been conducted in this regard, demonstrating that the structures can effectively intercept rockfall impact energies exceeding 5000 kJ (Lambert et al., 2009). Moreover, geosynthetic have proven to be efficacious in reducing wall stresses (Lu et al., 2021). This structure is characterized by a substantial spatial footprint and is associated with the risk of overturning during construction in steep terrain (Peila et al., 2007). Additionally, when the topography at the wall site features steep slopes, the available space behind the wall for accommodating rockfalls becomes constrained.

In response to the challenges posed by steep terrains, narrow site conditions, and suboptimal foundation conditions in mountainous terrain, Hu et al. (2019) introduced the PSRW structure. The structures are composed of a buffer layer and an anti-slip pile-slab structure. It has found widespread application in southwestern China (Fig. 1). Due to its implementation of pile foundations, this structure possesses characteristics such as a small footprint, high interception height, and ease of construction. However, the current PSRW design verification is to treat the structure as an underground continuous wall (Caghp, 2019). And, due to the composite nature of this structure, the dynamical response at various impact points remains ambiguous. The maximum impact energy that the structure can withstand has also not been thoroughly investigated. It can lead to potential underestimation of failure possibilities (Fig. 1d). At the same time, the existing research focuses on the single slab and pile impacted by rockfall (Wu et al., 2021; Yong et al., 2021).

Fig. 1. PSRW in south-western China (a) Kongyu town (b) Jiuzhaigou nature reserve (c) Zhenjiangguan tunnel exit in Chengdu-lanzhou railway (d) Wenchuan-Maerkang expressway.

https://doi.org/10.5194/egusphere-2023-2715
Preprint. Discussion started: 21 November 2023

Therefore, analysis of structural dynamic response and concrete damage is crucial to determine its effectiveness in mitigating rockfall hazards. Based on the research status, due to the unique advantages of the finite element method, this study uses the LS-DYNA to simulate the complete process of rockfall impact PSRW. This methodology has been widely adopted by numerous researchers and demonstrated as suitable for simulating impact problems of reinforced concrete structure (Zhong et al., 2022; Fan et al., 2022; Bi et al., 2023). In conclusion, a full-scale numerical model of a four-span pile-slab retaining wall satisfying specification requirements is established. The rationality of the selected material constitutive models and a numerical algorithm was validated by reproducing two physical model tests. The structure's dynamic behavior under different impact velocities and impact centers is discussed（Fig. 2). The results provide insights into sturcture dynamic response analysis of the PSRW and serve as a benchmark for further research.

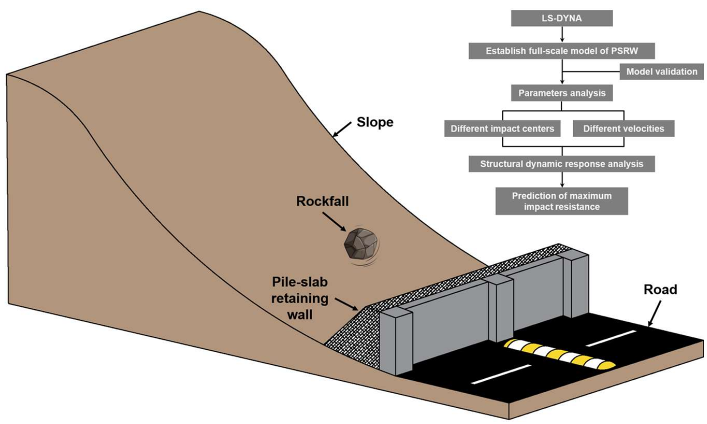

Fig. 2 Mind mapping.

2. Numerical model and validations

2.1. Model configuration

2.1.1. Engineering background

The design diagram of the PSRW (Fig. 3) adheres to the Chinese standard Code for the design of rock retaining wall engineering in geological hazards (Caghp, 2019). The anti-slide piles with a concrete protective layer thickness of 0.04 m have a cross-section area of 1.8 m × 1.25 m. The total pile length is 12 m, and the embedded section is 6 m. The HRB 400 longitudinal bar with diameters of 25 mm and 32 mm were arranged in the pile (Fig. 3c). The stirrups are HRB335 with a diameter of 16 mm and a spacing of 200 mm. The slabs between the piles are 6 m in length, 3.5 m in width, and 0.5 m in thickness. These slabs contain two layers of 16 mm-diameter reinforced bar. The sand buffer layer are 1 m and 5 m on top and bottom, respectively. A geogrid is horizontally placed in the buffer layer at 0.25 m intervals. Lastly, 1 m^3 sphere rock boulder with a diameter of 1.24 m was set as an impactor. The impact locations are 2#slab center (CS) and 3# pile center (CP) at 5.25 m over the ground.

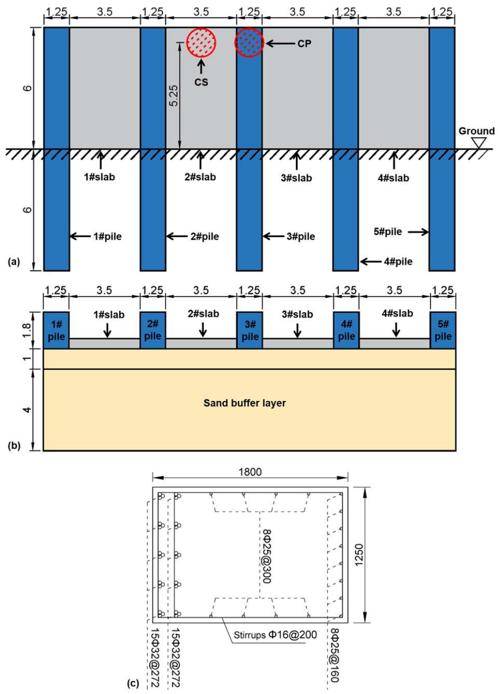

Fig. 3. The design diagram of PSRW (a) front view (unit: m) (b) top view (unit: m) (c) cross-sectional profile of pile (unit: mm).

2.1.2. *Soil-pile interaction*

Under the impact, the lateral deformations of the pile are greatly influenced by the plastic behavior of the soil, particularly the soil near the pile. Given their importance and complexity, it isn't easy to thoroughly describe soil-pile interactions. This paper calculates the pile-soil interaction by the lateral resistance-deflection (*p-y*) curve method. As state by Truong and Lehane (2018), the *p-y* curves for square cross-section pile are utilized as

$$\frac{P}{P_{\mathrm{u}}} = \tanh\left[5.45\left(\frac{y}{B}\right)^{0.52}\right] \tag{1}$$

https://doi.org/10.5194/egusphere-2023-2715
Preprint. Discussion started: 21 November 2023

$$\frac{P}{S_{\mathrm{u\_cu}}}=10.5\left[1-0.75e^{-0.6z/B}\right]S_{\mathrm{p}} \tag{2}$$

where P is the actual lateral soil resistance, kPa; P_{u} is the ultimate lateral soil resistance, kPa; $S_{\mathrm{u\_cu}}$ is consolidated isotropic undrained triaxial shear strength of soil, kPa/m; y is the actual lateral soil deformation, m; B is pile width, m; z is depth below the soil surface, m; S_{p} is a shape correction factor.

According to the reference and simulated model, the $S_{\mathrm{u\_cu}}$ and S_{p} are adopted as 1.5 kPa/m and 1.25, respectively. Besides, the soil is modeled by compressive inelastic springs, arranged every 0.25 m along the pile height and side (Fig. 4a).

2.1.3. Numerical model and numerical simulation scheme

(1) Numerical model

The numerical model of PSRW is shown in Fig. 4. The material constitutive models, unit types, physical-mechanical parameters, and parameter source for all components are listed in Table 1. The rationality of all material constitutive models and physical mechanics parameters were verified in Section 2.2. The both piles and buffer layers are fixed for the boundary conditions. Additionally, both sides of the buffer layer are blocked by infinitely rigid walls. The contact type between the rockfall, sand buffer layer and pile-slab structure were set to automatic surface-to-surface.

(2) Numerical simulation scheme

According to previous research (Muraishi et al., 2005; Chau et al., 2002), angular velocity of impactor was neglected in numerical simulations, and line velocities were set as 10, 15, 20, 25, and 30 m/s, corresponding to impact energies of 130, 292.5, 520, 812.5, and 1170 kJ (Table 2). The linear velocity is perpendicular to surface of the buffer layer.

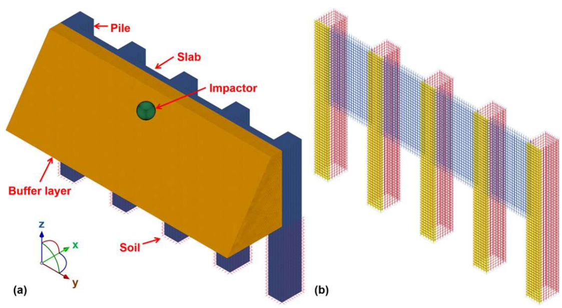

Fig. 4. Numerical model of the PSRW (a) numerical model (b) reinforced bar of PSRW (unit: mm).

https://doi.org/10.5194/egusphere-2023-2715
Preprint. Discussion started: 21 November 2023

Table 1 Material constitutive model and physical-mechanical parameters for various components of PSRW.

Items	Constrained model	Unit types	Integral methods	Density (kg/m^3)	Young's modul (MPa)	Poisson's ratio
Concrete	Continue cap concrete (MAT_159)(Heng et al., 2021)	Solid element	One integration point	2450	30000	0.3
Reinforced bar	Plastic kinematic model (MAT_003)(Heng et al., 2021)	Beam element	2×2 Gauss integration	7850	204000	0.3
Sand buffer layer	Soil-foam model (MAT_063)(Bhatti and Kishi, 2010)	Solid element	One integration point	1720	100	0.3
Impactor	Rigid body (MAT_020)	Solid element	One integration point	2600	20000	0.25
Geogrid	Plastic kinematic model (MAT_003)(Lee et al., 2010)	Shell element	Belytschko-Tsay integration	1030	464	0.3

Table 2 Detailed numerical simulation scheme.

Case	Impact location	Impact height (m)	Impact velocity (m/s)	Impact kinetic energy (kJ)
CP-V10			10	130
CP-V15			15	292.5
CP-V20	3# pile center		20	520
CP-V25			25	812.5
CP-V30		5.25	30	1170
CS-V10			10	130
CS-V15			15	292.5
CS-V20	2# slab center		20	520
CS-V25			25	812.5
CS-V30			30	1170

Note: CP denotes the 3# pile center as impact location; CP denotes the 2# slab center as impact location; V denotes the velocities of rockfall.

2.2. Model validation

In order to verify the rationality of the selected material constitutive model and the established numerical model. Two physical model tests from previously published papers (Heng et al., 2021; Demartino et al., 2017; Schellenberg, 2008) were selected to reproduce.

2.2.1. Failure test of RC cantilever column

The physical model test conducted by Demartino et al. (2017) was selected to verify the ability of constitutive model to reflect the accumulative damage for RC structures under impact loads. The model is composed of a cylindrical column with a diameter of 0.3 m and a height of 1.7 m, and a square-section concrete foundation with length of 0.9 m and height of 0.5 m. The column was reinforced with sixteen 8 mm diameter longitudinal reinforced bar and 6.5 mm diameter stirrups at 100 mm spacing. The foundation was firmly connected to the ground using four 50 mm diameter high-strength prestressed reinforced bar. The experiment involved a test truck made of Q235 steel

https://doi.org/10.5194/egusphere-2023-2715
Preprint. Discussion started: 21 November 2023

(considered as a rigid body) with 1.55 m in length, 1.35 m in width, and 0.59 m in height. Attached to the truck was an impact hammer measuring 0.58 m in length, 0.2 m in width, and 0.08 m in thickness (Fig. 5a). The impactor was positioned 0.4 m above the bottom of the column and was released at a velocity of 3.02 m/s (impact energy of 7.21 kJ). Fig. 5b shows the numerical model with hexahedral mesh. The material constitutive models for components are shown in Table 1. For the boundary conditions, the model was fixed with four high-strength bolts.

The trend and amplitude of the impact forces by numerical simulations closely matched the experimental results (Fig. 6). Similarly, Table 3 indicates consistency between the degrees of the experimental and numerical damage of concrete. The deviations of peak impact forces between the numerical simulations and the experiments were below 10% (Table 4). These results suggest that the numerical model and its controlling parameters can reliably simulate the accumulative damage to RC structures under impact loads. According to the accuracy and computational time, a mesh size model of 50 mm was adopted for the numerical simulations in this study.

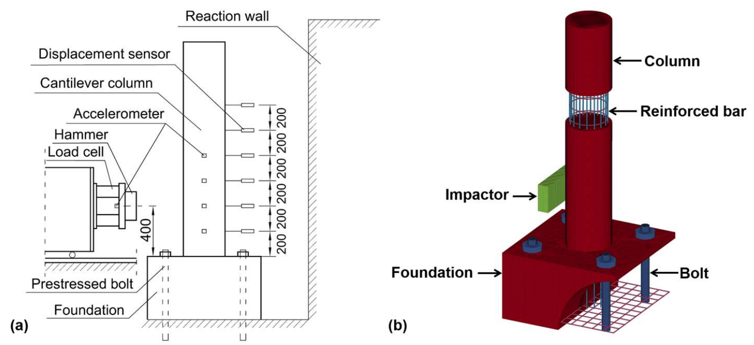

Fig. 5. Model of RC cantilever column failure test
(a) experimental model (b) numerical model (unit: mm).

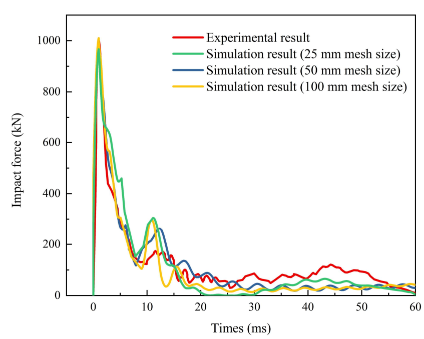

Fig. 6. Dynamic curve of impact force with different mesh size.

https://doi.org/10.5194/egusphere-2023-2715
Preprint. Discussion started: 21 November 2023

Table 3 Comparison of experimental and simulation results of concrete damage accumulation with time.

Time(ms)	7.5	10	15	20	50
Experimental results(Demartino et al., 2017)	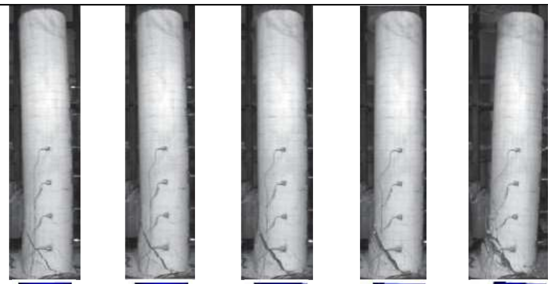				
Simulation results	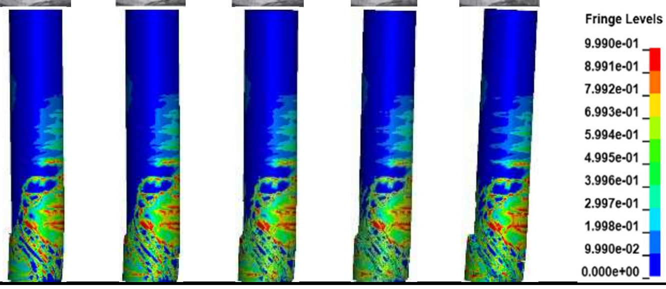				

Table 4 Simulation results of different mesh sizes.

Items	Impact force (KN)	Displacement of column at 1.2m height (mm)	Number of the element	Computational time (hour)
Physical model test	999.52	22.3	/	/
25 mm mesh size	966.72	23.1	5462900	24
50 mm mesh size	978.1	22	807534	4.2
100 mm mesh size	1009.35	21.3	172268	1.2

2.2.2. *Failure test of RC slab with a buffer layer*

The physical model test conducted by Schellenberg (2008) was selected to verify the function of the constitutive model to reflect the interaction between the boulder, sand buffer layer, and RC structure. The specimen comprises a RC slab measuring 1.5 m × 1.5 m × 0.23 m and a sand buffer layer with 0.5 m in radius and 0.45m in thickness (Fig. 7). The slab is reinforced with one layer of reinforced bar with 12 mm diameter and a spacing of 95/45 mm for the lower layer. Boulder diameter and density (considered a rigid body) is 0.8 m and 3110 kg/m^3. The impact position is at the center of the buffer layer, with an impactor velocity of 5.5 m/s (impact energy of 14.4kJ). The material constitutive models for concrete, reinforced bar, and sand buffer layer are shown in Table 1. For the Boundary conditions, the bottom of the supports was fixed.

Fig. 8 presents the dynamic curve of impact force, slab center displacement, and center reinforced bar axial strain. The results demonstrate that the deviations of the peak impact force, the maximum strain of the reinforced bar, and the slab center displacement are less than 10%. Therefore,

https://doi.org/10.5194/egusphere-2023-2715
Preprint. Discussion started: 21 November 2023

the numerical model and its controlling parameters can reliably simulate sand cushion layer, and RC structure under impact loads.

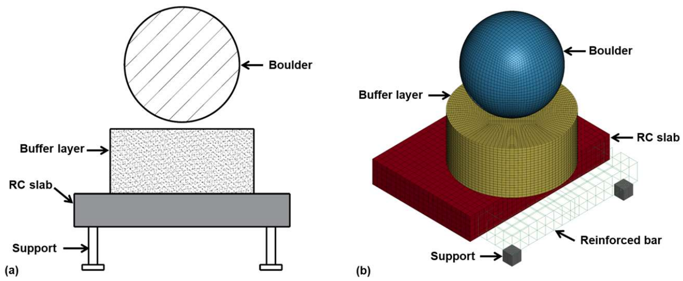

Fig. 7. Model of RC slab failure test
(a) experimental model (b) numerical model (unit: mm).

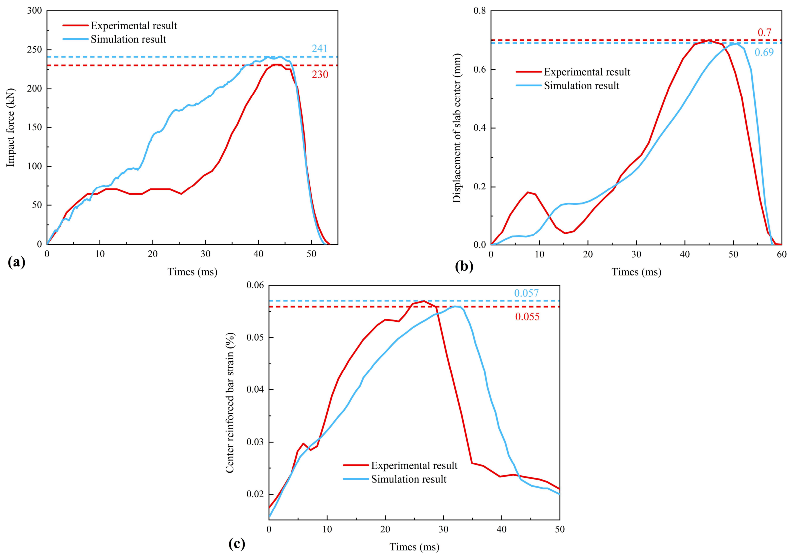

Fig. 8. Comparisons between experimental and simulation results
(a) impact force (b) displacement of slab center (c) axial strain of reinforced bar.

3. Numerical results

In this section, the dynamic response of PSRW under different impact centers and different impact velocities are compared and analyzed. The main evaluation xxes are as follows: impact force (the contact force between the impactor and the buffer layer), interaction force (the contact force between the buffer layer and the RC structure), stress of concrete and reinforced bar, concrete damage, lateral displacement at the crown of different components (piles and slabs), and lateral displacement of all piles at the ground surface.

https://doi.org/10.5194/egusphere-2023-2715
Preprint. Discussion started: 21 November 2023

3.1. *Influence of different impact centers*

To analyze the influence of dynamic behaviors of PSRW under different impact centers, two group simulations under maximum impact energy (CP-V30 and CS-V30) are selected for comparison.

3.1.1. *Impact force and interaction force*

Fig. 9a and b show the dynamic curves of the impact force and interaction force, respectively. Both force curves exhibit a distinct single-peaked pattern. The impact force rapidly reduces to zero due to the energy-dissipating properties of the sand buffer layer (Fig. 9a). In contrast, the interaction force remains at a non-zero value (475 kN) (Fig. 9b). Due to the permanent deformation of the structure, and the gravity component of the sand buffer acts on the surface of the structure. Furthermore, Fig. 9a illustrates the close overlap of the impact forces for various impact centers, depending on the buffer and impactor characteristics, and minimally affected by the impact center. The slight differences observed in the dynamic curve of interaction force under CP-V30 and CS-V30 may be attributed to the flexural stiffness of the slab and pile .

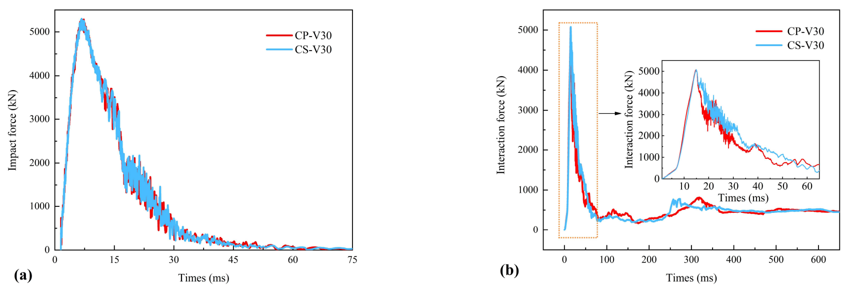

Fig. 9. Dynamic curves of impact force and interaction force under various impact centers (a) impact force (b) interactional force.

3.1.2. *Stress of concrete*

The minimum principal stress of concrete and the effective stress of reinforced bar are important indexes to evaluate the dynamic response of RC structures (Zhong et al., 2021; Zhong et al., 2022). Fig. 10 shows the minimum principal stress nephogram of concrete under CP-V30 from 1 to 650 ms. When t = 1 ms (Fig. 10a), the maximum stress focus on the bottom of the piles. When t = 14.7 ms (Fig. 10b), the minimum principal stress of concrete around the impact point increased rapidly to 7.421 MPa. When t= 22.8 ms (Fig. 10c), the concrete elements at the joints of the 3# pile and slabs achieve compressive strengt, leading to concrete damage. When t= 650 ms (Fig. 10d), the

https://doi.org/10.5194/egusphere-2023-2715
Preprint. Discussion started: 21 November 2023

total volume of damaged elements reaches 0.63 m^3, which occupies a proportion of 0.35%. The concrete damage nephogram (Fig. 10a) shows that the concrete damage is mainly concentrated at the joints of pile and slab under CP-V30.

Fig. 12 shows the minimum principal stress nephogram of concrete under CP-V30 from 1 to 650 ms. When t = 1 ms, the maximum stress focus on the bottom of the piles (Fig. 12a). When t = 14.7 ms, the minimum principal stress around the impact point increased rapidly to 12.117 MPa (Fig. 12b). When t = 22.4 ms, the elements of the concrete at the impact point of the 2# slab achieve ultimate compressive strengt, leading to the concrete damage (Fig. 12c). When t = 650 ms, the total volume of damage elements reaches 0.61 m^3 (Fig. 12d), which occupies a proportion of 0.34 %. Notably, the concrete damage is mainly concentrated at the 2# slab and the joints of piles and slabs under CS-V30 (Fig. 11b).

The dynamic impact process of PSRW includes: the impact force was transmitted to the overall RC structure through the buffer layer after the impact. Simultaneously, stress spread around and covered the entire RC structure at the corresponding impact height point, leading to deformation and damage of the structure.

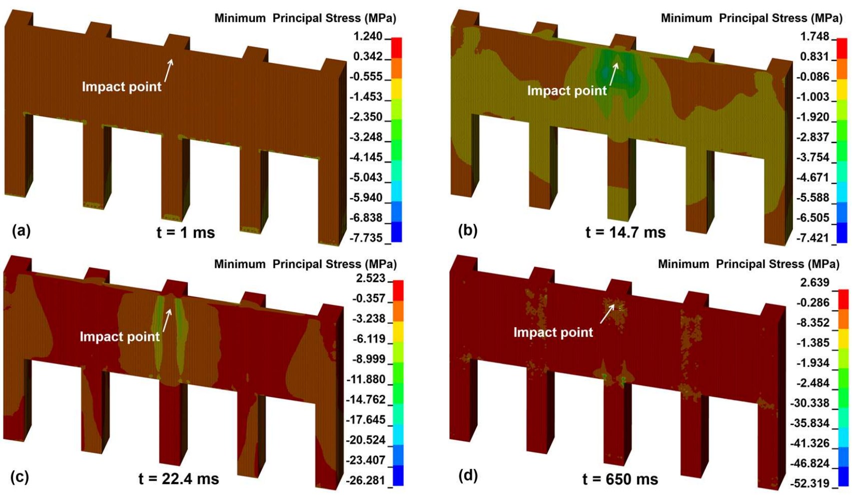

Fig. 10. Concrete minimum principal stress nephogram under CP-V30.

https://doi.org/10.5194/egusphere-2023-2715
Preprint. Discussion started: 21 November 2023

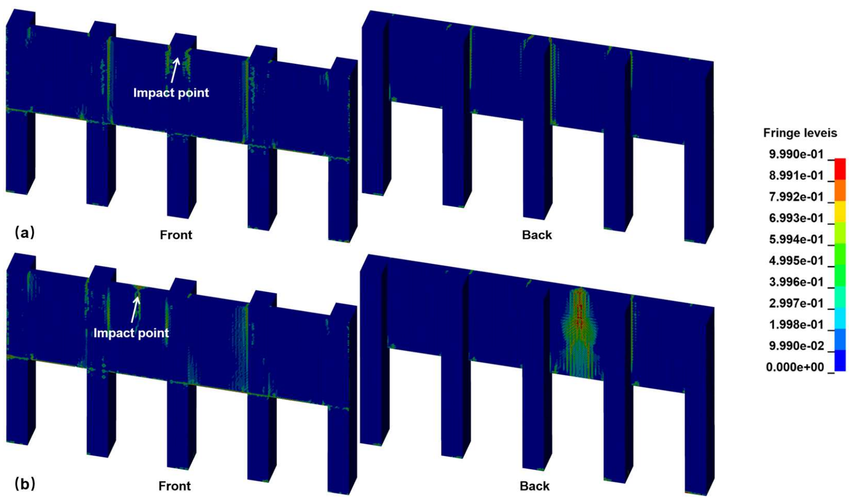

Fig. 11. Concrete damage nephogram at t = 650 ms (a) CP-V30 (b) CS-V30.

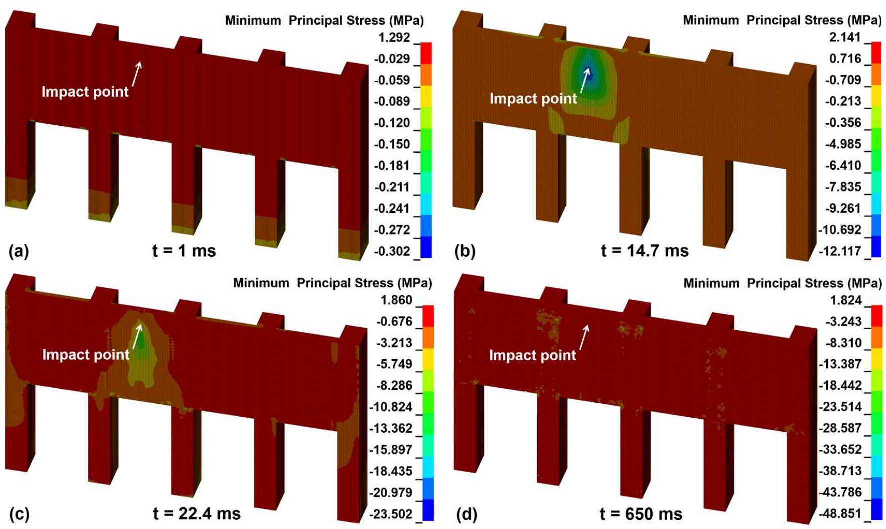

Fig. 12. Concrete minimum principal stress nephogram under CS-V30.

3.1.3. Stress of reinforce bar

Fig. 13 shows the effective stress nephogram of the reinforced bar from 1 to 650 ms under the condition of CP-V30. It can be observed that: (i) when t = 1 ms, the greatest stress concentrated at the bottom of the pile (Fig. 13a); (ii) when t = 14.7 ms (the moment of attaining the maximum interaction force), the maximum stress concentrated at the vicinity of the impact point and the joints of piles and slabs (Fig. 13c); (iii) when t = 650 ms, the maximum stress concentrated at the longitudinal bar of 2#, 3#, and 4# pile (Fig. 13d). Moreover, the effective stress of reinforced bar

https://doi.org/10.5194/egusphere-2023-2715
Preprint. Discussion started: 21 November 2023

did not exceed the ultimate yield stress.

Fig. 14 shows the effective stress nephogram of reinforced bar from 1 to 650 ms under CS-V30. It can be observed that: (i) when t = 1 ms, the greatest stress concentrated at the bottom of the pile (Fig. 14a); (ii) when t = 14.7 ms, the effective stress of reinforced bar around the impact point increased rapidly to 137.2 MPa. (Fig. 14c); (iii) when t = 650 ms, the maximum stress concentrated at the longitudinal bar of 2#, 3#, and 4# pile (Fig. 14d). Moreover, the effective stress of reinforced bar did not exceed the ultimate yield stress.

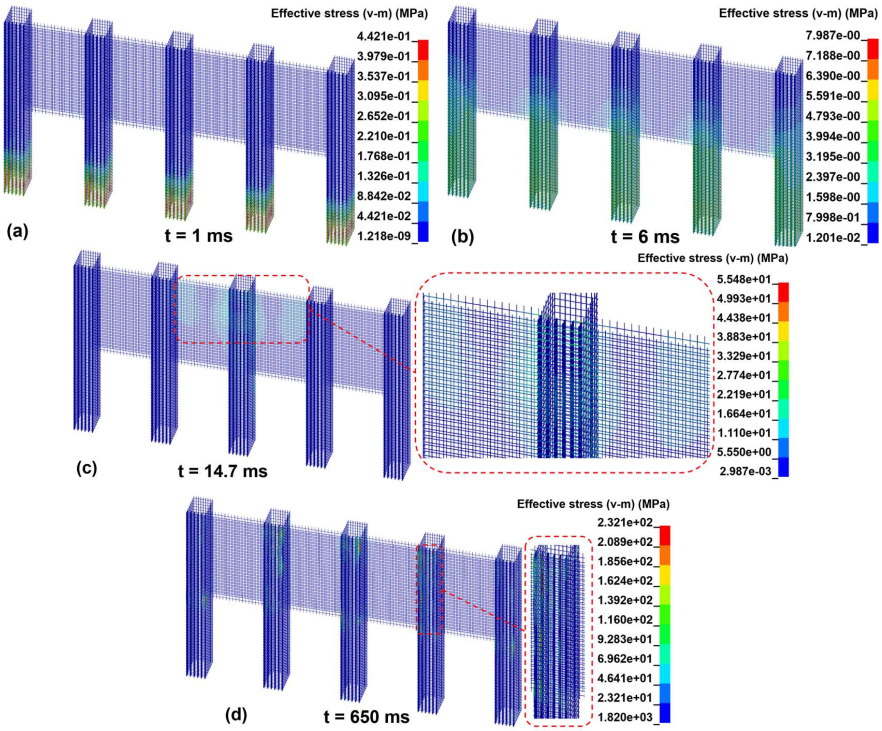

Fig. 13. Reinforced bar effective stress nephogram under CP-V30.

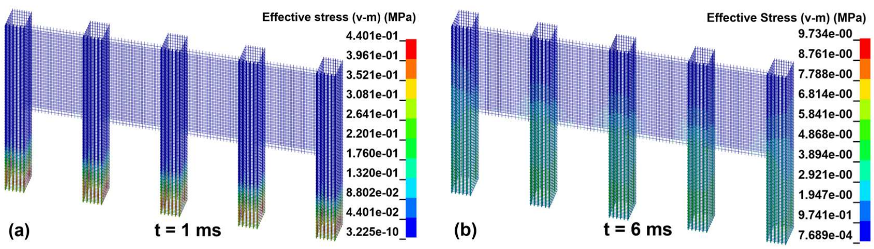

https://doi.org/10.5194/egusphere-2023-2715
Preprint. Discussion started: 21 November 2023

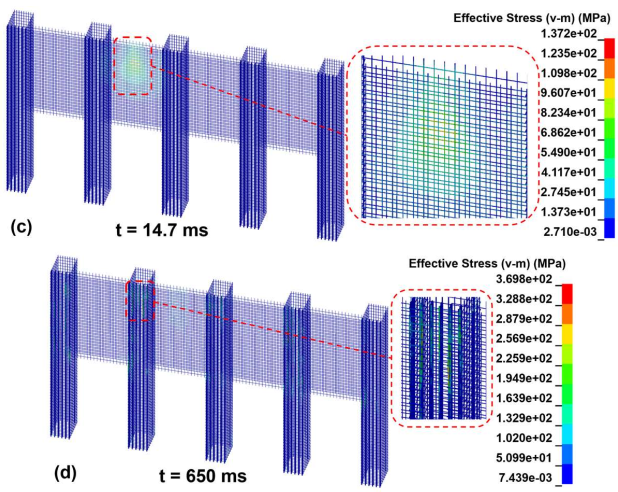

Fig. 14. Reinforced bar effective stress nephogram under CS-V30.

3.1.4. Lateral displacement at the crown of different components

Fig. 15a presents a scatter plot illustrating the temporal variation of lateral displacements at the crown of different components under CP-V30 and CS-V30. The lateral displacement rapidly increased till t = 177 ms and gradually decreased until t = 650 ms. The final displacement does not reach 0, indicating plastic deformation of both the pile and the slab. Comparing the displacement under CS-V30 and CP-V30 (Fig. 15), the trends are consistent, but the magnitude differs. This discrepancy can be attributed to the greater deformation capacity of slab rather than pile under the same impact energy.

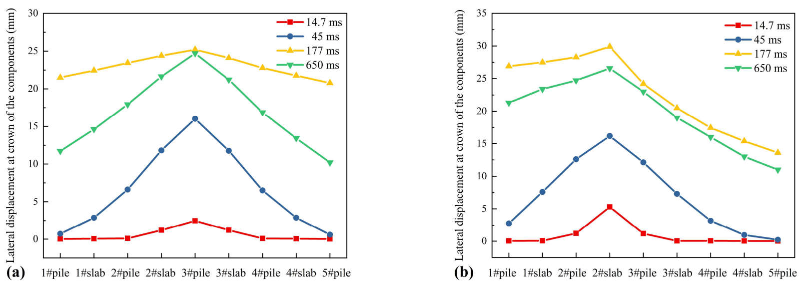

Fig. 15. Lateral displacement at crown of the components (a) CP-V30 (b) CS-V30.

3.1.5. Lateral displacement of piles at the ground surface

Fig. 16a and b show the dynamic curve of lateral displacement of all piles at the ground surface under CP-V30 and CS-V30, respectively. Under CP-V30, the 3# pile exhibited the maximum lateral displacement, whereas the 2# pile exhibited the maximum lateral displacement under CS-V30. This is because under the CS-V30, the structural asymmetry on both sides of the impact center grants

https://doi.org/10.5194/egusphere-2023-2715
Preprint. Discussion started: 21 November 2023

one side of 2# pile greater freedom, leading to the greater lateral displacement. By comparing the lateral displacement of 2# pile under CS-V30 and 3# pile under CP-V30 (Fig. 16c), it indicates that the maximum lateral displacement of pile at the ground surface is greater under CP conditions with the same impact velocity. The characteristics of the lateral displacements is attributed to that the concrete slab can deform large and absorb more energy.

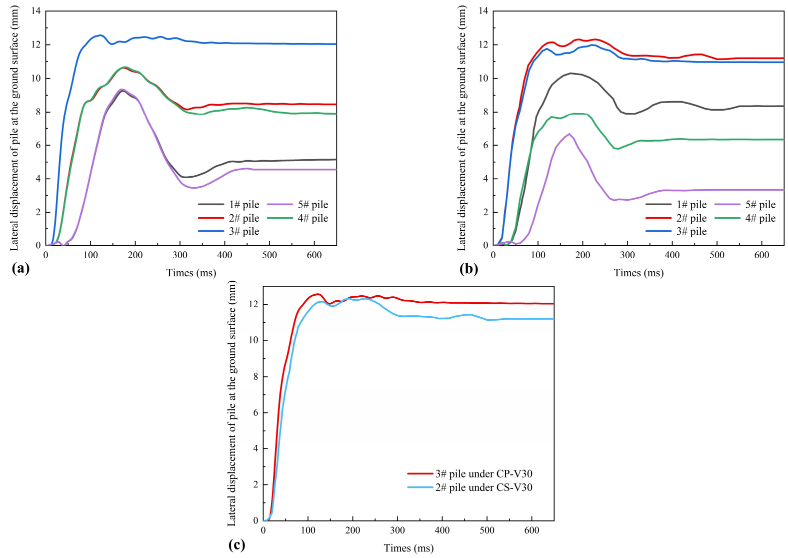

Fig. 16. Dynamic curves of lateral displacement of pile at the ground surface
(a) CP-V30 (b) CS-V30 (c) compare between CP-V30 and CS-V30.

3.2. Influence of different impact velocities

Fig. 17 shows the impact force, interaction force, and lateral displacement of 3# pile at the ground surface enlarge as the impact velocity increases under CP. When the velocity increases from 15 m/s to 30 m/s, the impact force increases by 1.42, 1.91, and 2.41 times, the interaction force increases by 1.25, 1.47, and 1.68 times, and the lateral displacement of 3# pile at ground surface increases by 1.57, 2.24, and 3 times at t = 650 ms.

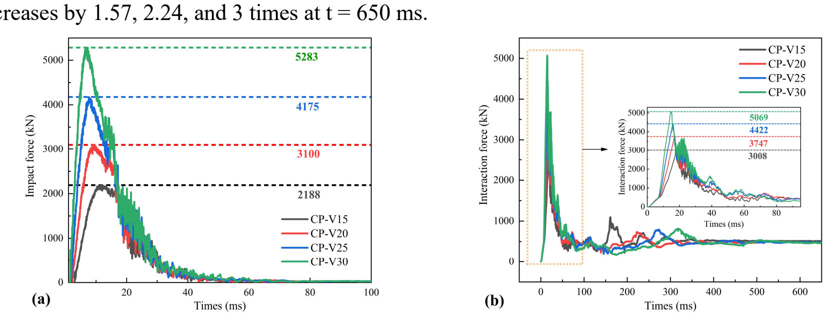

https://doi.org/10.5194/egusphere-2023-2715
Preprint. Discussion started: 21 November 2023

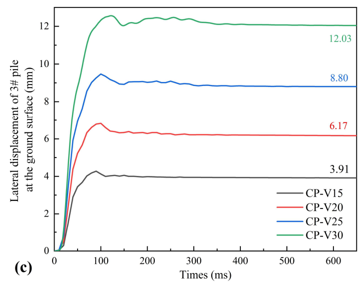

Fig. 17. Dynamic curves of evaluation indexes under various velocities
(a) impact force (b) interactional force (c) lateral displacement at the ground surface of 3# pile.

Fig. 18 shows the impact force, interaction force, and lateral displacement of 2# pile at the ground surface enlarge as the impact velocity increases under CS. When the velocity increases from 15 m/s to 30 m/s, the impact force increases by 1.41, 1.90, and 2.41 times, the interaction force increases by 1.24, 1.47, and 1.68 times, and the lateral displacement of 3# pile at ground surface increases by 1.55, 2.23, and 3 times at t = 650 ms.

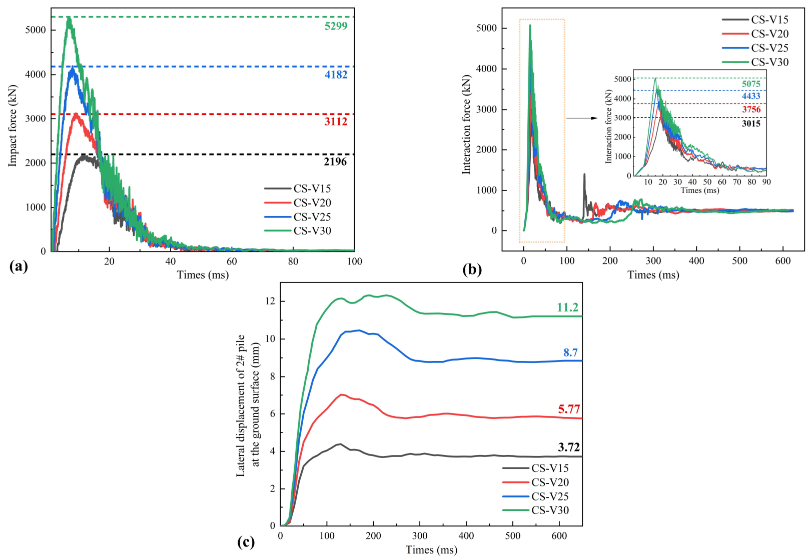

Fig. 18. Dynamic curves of evaluation indexes under various velocities
(a) impact force (b) interactional force (c) lateral displacement at the ground surface of 3# pile.

4. Discussions

Table 5 lists the initial kinetic energy of impactor (E), the peak impact force (F_{dm}), the peak interaction force (F_{im}), the ratio of the peak impact force to the peak interaction force (α), the maximum the lateral displacement of pile at the ground surface at t = 650 ms (S_{mpt}), the number of damage failure units (N_d), and the ratio of damage failure units to overall RC structure units (β).

https://doi.org/10.5194/egusphere-2023-2715
Preprint. Discussion started: 21 November 2023

Table 5 Simulation results for various impact cases.

Case	E (kJ)	F_{dm} (kN)	F_{im} (kN)	α (%)	S_{mpt} (mm)	N_d	β (%)
CP-V10	130	1420	2170	65.4	2.25	83	0.0059
CP-V15	292.5	2188	3008	72.7	3.91	817	0.0577
CP-V20	520	3100	3747	82.7	6.17	2179	0.1539
CP-V25	812.5	4175	4422	94.4	8.8	3088	0.2181
CP-V30	1170	5283	5069	104.2	12.03	5040	0.3559
CS-V10	130	1426	2182	65.4	1.76	52	0.0037
CS-V15	292.5	2196	3015	72.7	3.72	321	0.0227
CS-V20	520	3112	3756	82.7	5.77	1062	0.0750
CS-V25	812.5	4182	4433	94.4	8.7	2728	0.1927
CS-V30	1170	5299	5075	104.2	11.2	4880	0.3446

Under the premise of known impact energy, estimating impact force, interaction force, and displacement for the structural design is very important. As shown in Table 5, the difference of peak impact force (F_{dm}) with different impact centers is minimal, so that CP simulation results were selected to analyze. The dependence of the peak impact force on the impact energy is shown in Fig. 19a, with a correlation coefficient R^2 = 0.99, i.e.,

$$F_{dm} = 3.69(E + 290.33) = 1845(mv^2 + 0.58) \tag{1}$$

where m is the impactor mass, t (m= 2.6 therein), v is the initial impact velocity, m/s (10 m/s ⩽ v ⩽ 30 m/s herein).

The dependence of the ratio of peak impact force to peak interaction force on the impact energy is shown in Fig. 19b, with a correlation coefficient of 0.99, i.e.,

$$\alpha = 0.037(E + 1671.89) = 18.5(mv^2 + 3.34) \tag{2}$$

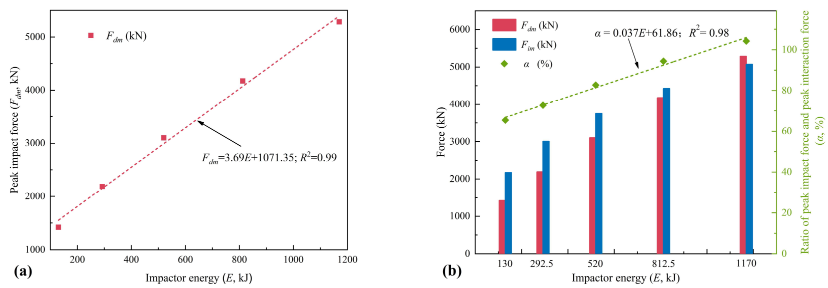

Fig. 19. Dependence of various indexes on impactor energy (a) peak impact force (b) the ratio of peak impact force and peak interaction force.

The lateral displacement of pile at the ground surface is an important index to judge the failure of pile foundation under lateral load. As shown in Table 5, the maximum lateral displacement of pile at the ground surface under pile as impact center is greater than that under slab as impact center. Therefore, the situation where the pile is the center of impact is the more dangerous. As shown in Fig. 20, with the increase of impact energy, the displacement value and number of damage failure

https://doi.org/10.5194/egusphere-2023-2715
Preprint. Discussion started: 21 November 2023

units enlarges, which means the structure suffers more damage under CP. Furthermore, the maximum lateral displacement of pile at the ground surface when t = 650 ms, can be calculated by the following aquation:

$$S_{mpt} = 0.00934\left(E + 164.88\right) = 4.67\left(mv^2 + 0.33\right) \tag{3}$$

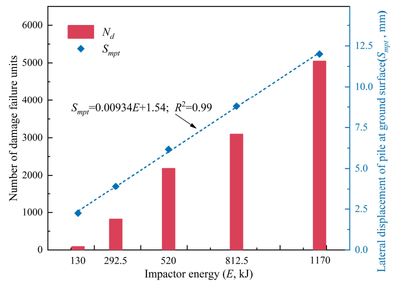

Fig. 20. Dependence of the lateral displacement of 3# pile at the ground surface on impactor energy

According to the Chinese standard Code for the Design of Rock Retaining Wall Engineering in Geological Hazards (Caghp, 2019), the lateral displacement of the resistant sliding pile at the ground surface must not exceed 10 mm. Substituting this value into Formula 3, the maximum impact energy that the PSRW can withstand in this study is 905 kJ. The maximum impact energy of the structure established in this paper is much higher than that of the traditional RC retaining walls (500 kJ)(Maegawa et al., 2011). Notably, if the impact position is at the lower sections of the pile and slab, the PSRW can withstand more impact energy. Due to the advantage of pile foundation, the structure occupies a smaller area than traditional RC rock retaining walls and can be arranged in the steep slopes. According to the numerical results, under a higher-energy impact of rockfall, the joints of pile and slab, slab thickness and buffer thickness should be optimized to avoid damages and reduce lateral displacements.

5. Conclusion

Numerical experiments of PSRW under impact were performed to comprehensively analyze the impact force, interaction force, stress of concrete and reinforced bar, concrete damage, and the lateral displacements. The main conclusions drawn are as follows:

(1) Concrete damage mainly concentrates at the joints between piles and slabs, the impact position, and the section of piles at the ground surface. Therefore, in order to reduce structural concrete damage, these focal sections should be initially considered for structural optimization.

(2) Under various impact center conditions, the difference of impact force and interaction force is very small. However, when the pile serves as the impact center, lateral displacement of pile at the ground surface and concrete damage are greater, which illustrates that the pile as the impact center is a more dangerous impact situation.

(3) Structural evaluation indexes, including the impact force, the ratio of peak impact force to peak interaction force, and maximum lateral displacement of pile at the ground surface, increase with the growth of impact energy. These relationships can provide assessments for impact forces, interaction force, and lateral displacement of pile at the ground surface in PRSW structural design. According to the relationship between the impact energy and lateral displacement of pile at the ground surface, the maximum impact energy that the PSRW can withstand in this study is 905 kJ when the structure top is taken as the impact point.

CRediT authorship contribution statement

Peng Zou: Methodology, Simulation, Visualization, Writing - original draft. **Gang Luo:** Tests design, editing, funding acquisition, writing - review. **Yuzhang Bi:** Visualization, Writing - review, editing. **Hanhua Xu:** Writing - review, editing.

Declaration of Competing Interest

The authors declare that they have no known competing financial interests or personal relationships that could have appeared to influence the work reported in this paper.

Acknowledgments

This research was funded by the National Natural Science Foundation of China (42277143), the National Key R&D Program of China (2022YFC3005704), and the Science and the research project of the Department of Natural Resources of Sichuan Province (KJ-2023-004, KJ-2023-029).

https://doi.org/10.5194/egusphere-2023-2715
Preprint. Discussion started: 21 November 2023

References

Bhatti, A. Q. and Kishi, N.: Impact response of RC rock-shed girder with sand cushion under falling load, Nuclear Engineering and Design, 240, 2626-2632, https://doi.org/10.1016/j.nucengdes.2010.07.029, 2010.

Bi, Y., Li, M., Wang, D., Zheng, L., Yan, S., and He, S.: A numerical study of viscous granular flow in artificial step-pool systems: flow characteristics and structure optimization, Acta Geotechnica, https://doi.org/10.1007/s11440-023-01933-1, 2023.

CAGHP: Code for design of rock retaining wall engineering in geological hazards (T/CAGHP060-2019), China University of Geosciences Press, Wuhan2019. (in Chinese)

Chau, K. T., Wong, R., and Wu, J.: Coefficient of restitution and rotational motions of rockfall impacts, International Journal of Rock Mechanics and Mining Sciences, 39, 69-77, https://doi.org/10.1016/S1365-1609(02)00016-3, 2002.

Crosta, G. and Agliardi, F.: Parametric evaluation of 3D dispersion of rockfall trajectories, Natural Hazards and Earth System Sciences, 4, 583-598, https://doi.org/10.5194/nhess-4-583-2004, 2004.

Demartino, C., Wu, J. G., and Xiao, Y.: Response of shear-deficient reinforced circular RC columns under lateral impact loading, International Journal of Impact Engineering, 109, 196-213, https://doi.org/10.1016/j.ijimpeng.2017.06.011, 2017.

Fan, W., Zhong, Z., Huang, X., Sun, W., and Mao, W.: Multi-platform simulation of reinforced concrete structures under impact loading, Engineering Structures, 266, 114523, https://doi.org/10.1016/j.engstruct.2022.114523, 2022.

Giani, G. P.: Rock slope stability analysis, CRC Press1992.

Heng, K., Li, R., Li, Z., and Wu, H.: Dynamic responses of highway bridge subjected to heavy truck impact, Engineering Structures, 232, 11828-11850, https://doi.org/10.1016/j.engstruct.2020.111828, 2021.

Hu, X., Mei, X., Yang, Y., and Luo, G.: Dynamic Response of Pile-plate Rock Retaining Wall under Impact of Rockfall, Journal of Engineering Geology, 27, 123-133, 2019. (in Chinese)

Hungr, O., Leroueil, S., and Picarelli, L.: The Varnes classification of landslide types, an update, Landslides, 11, 167-194, https://doi.org/10.1007/s10346-013-0436-y, 2014.

Lambert, S., Gotteland, P., and Nicot, F.: Experimental study of the impact response of geocells as components of rockfall protection embankments, Natural Hazards and Earth System Sciences, 9, 459-467, https://doi.org/10.5194/nhess-9-459-2009, 2009.

Lee, K., Chang, N., and Ko, H.: Numerical simulation of geosynthetic-reinforced soil walls under seismic shaking, Geotextiles and Geomembranes, 28, 317-334, https://doi.org/10.1016/j.geotexmem.2009.09.008, 2010.

Lu, L., Lin, H., Wang, Z., Xiao, L., Ma, S., and Arai, K.: Experimental and numerical investigations of reinforced soil wall subjected to impact loading, Rock Mechanics and Rock Engineering, 54, 5651-5666, https://doi.org/10.1007/s00603-021-02579-9, 2021.

Maegawa, K., Yokota, T., and Van, P. T.: Experiments on rockfall protection embankments with geogrids and cushions, GEOMATE Journal, 1, 19-24, 2011.

Mavrouli, O., Giannopoulos, P., Carbonell, J. M., and Syrmakezis, C.: Damage analysis of masonry structures subjected to rockfalls, Landslides, 14, 891-904, https://doi.org/10.1007/s10346-016-0765-8, 2017.

Muraishi, H., Samizo, M., and Sugiyama, T.: Development of a flexible low-energy rockfall protection

https://doi.org/10.5194/egusphere-2023-2715
Preprint. Discussion started: 21 November 2023

fence, Quarterly Report of RTRI, 46, 161-166, https://doi.org/10.2219/rtriqr.46.161, 2005.

Peila, D. and Ronco, C.: Design of rockfall net fences and the new ETAG 027 European guideline, Natural Hazards and Earth System Sciences, 9, 1291-1298, https://doi.org/10.5194/nhess-9-1291-2009, 2009.

Peila, D., Oggeri, C., and Castiglia, C.: Ground reinforced embankments for rockfall protection: design and evaluation of full scale tests, Landslides, 4, 255-265, https://doi.org/10.1007/s10346-007-0081-4, 2007.

Perera, J. S., Lam, N., Disfani, M. M., and Gad, E.: Experimental and analytical investigation of a RC wall with a gabion cushion subjected to boulder impact, International Journal of Impact Engineering, 151, 103823-103839, https://doi.org/10.1016/j.ijimpeng.2021.103823, 2021.

Schellenberg, K.: On the design of rockfall protection galleries, ETH Zurich, 2008.

Shen, W., Zhao, T., Dai, F., Jiang, M., and Zhou, G. G.: DEM analyses of rock block shape effect on the response of rockfall impact against a soil buffering layer, Engineering Geology, 249, 60-70, https://doi.org/10.1016/j.enggeo.2018.12.011, 2019.

Truong, P. and Lehane, B.: Effects of pile shape and pile end condition on the lateral response of displacement piles in soft clay, Géotechnique, 68, 794-804, https://doi.org/10.1680/jgeot.16.P.291, 2018.

Volkwein, A., Schellenberg, K., Labiouse, V., Agliardi, F., Berger, F., Bourrier, F., Dorren, L. K., Gerber, W., and Jaboyedoff, M.: Rockfall characterisation and structural protection–a review, Natural Hazards and Earth System Sciences, 11, 2617-2651, https://doi.org/10.5194/nhess-11-2617-2011, 2011.

Wu, J., Ma, G., Zhou, Z., Mei, X., and Hu, X.: Experimental Investigation of Impact Response of RC Slabs with a Sandy Soil Cushion Layer, Advances in Civil Engineering, 2021, 1-18, https://doi.org/10.1155/2021/1562158, 2021.

Yang, J., Duan, S., Li, Q., and Liu, C.: A review of flexible protection in rockfall protection, Natural Hazards, 99, 71-89, https://doi.org/10.1007/s11069-019-03709-x, 2019.

Yong, A. C., Lam, N. T., and Menegon, S. J.: Closed-form expressions for improved impact resistant design of reinforced concrete beams, Structures, 29, 1828-1836, https://doi.org/10.1016/j.istruc.2020.12.041, 2021.

Yong, A. C., Lam, N. T., Menegon, S. J., and Gad, E. F.: Experimental and analytical assessment of flexural behavior of cantilevered RC walls subjected to impact actions, Journal of Structural Engineering, 146, 04020034, https://doi.org/10.1061/(ASCE)ST.1943-541X.0002578, 2020.

Yu, Z., Luo, L., Liu, C., Guo, L., Qi, X., and Zhao, L.: Dynamic response of flexible rockfall barriers with different block shapes, Landslides, 18, 2621-2637, https://doi.org/10.1007/s10346-021-01658-w, 2021.

Zhao, P., Xie, L., Li, L., Liu, Q., and Yuan, S.: Large-scale rockfall impact experiments on a RC rock-shed with a newly proposed cushion layer composed of sand and EPE, Engineering Structures, 175, 386-398, https://doi.org/10.1016/j.engstruct.2018.08.046, 2018.

Zhong, H., Lyu, L., Yu, Z., and Liu, C.: Study on mechanical behavior of rockfall impacts on a shed slab based on experiment and SPH–FEM coupled method, Structures, 33, 1283-1298, https://doi.org/10.1016/j.istruc.2021.05.021, 2021.

Zhong, H., Yu, Z., Zhang, C., Lyu, L., and Zhao, L.: Dynamic mechanical responses of reinforced concrete pier to debris avalanche impact based on the DEM-FEM coupled method, International Journal of Impact Engineering, 167, 104282-104301, https://doi.org/10.1016/j.ijimpeng.2022.104282, 2022.